INTEGRATED GEOPHYSICAL DATA FOR SWEET SPOT IDENTIFICATION IN BALTIC BASIN, POLAND

Kamil CICHOSTĘPSKI[1], Anna KWIETNIAK[1], Jerzy DEC[1], Monika KASPERSKA[1] & Kaja PIETSCH[1]

[1] *AGH University of Science and Technology in Krakow,*
Faculty of Geology, Geophysics and Environmental Protection, Department of Geophysics,
al. Mickiewicza 30, 30-059, Kraków, Poland; e-mails: kcichy@agh.edu.pl,
anna.kwietniak@agh.edu.pl, geodec@agh.edu.pl, krol@agh.edu.pl, pietsch@agh.edu.pl

Cichostępski, K., Kwietniak, A., Dec, J., Kasperska, M. & Pietsch, K., 2019. Integrated geophysical data for sweet spot identification in Baltic Basin, Poland. *Annales Societatis Geologorum Poloniae*, 89: 215–231.

Abstract: In the paper, the authors present the results of seismic reservoir characterization of shale gas deposits of the Lower Silurian and Ordovician (Sasino Formation and Jantar Formation), which are localized within the onshore part of the Baltic Basin, N Poland. For this purpose, acoustic inversion of seismic data and petrophysical analysis of well-log data were incorporated. The new approach that the authors used for acoustic inversion was the resolution enhancement algorithm, known as spectral blueing, before proceeding with the acoustic inversion process. The spectral blueing procedure enhances the seismic spectrum by weighting it with the well reflectivity spectrum. The resulting enhanced seismic volume manifests itself in higher energies of the high frequency component, while keeping the frequency range constant. With the results of acoustic inversion after the spectral blueing procedure, the authors were able to define two more potential exploration sites within the Ordovician deposits.

Key words: Shale plays, sweet spots, seismic inversion, resolution enhancement, Poland, Baltic Basin.

INTRODUCTION

The methods for gas prospecting in conventional targets should not be applied straightforwardly to unconventional reservoirs. In the case of the unconventional reservoir, it is not required that the trap contains a defined geometrical structure, within which hydrocarbons are distributed according to their densities. Unconventional reservoirs are for the most part highly compacted layers of often insignificant thicknesses and low permeability that can extend over wide areas. To be designated potential exploration sites such deposits must have a high kerogen content, expressed as the total organic content (TOC). Accordingly, it is of major importance to obtain information about the distribution of the petrophysical parameters and relate them to the seismic data.

High resolution well data provide information about the petrophysical properties in one dimension only. To define the spatial distribution of petrophysical properties seismic data are required. The interpreted seismic parameters (arrival times of reflected waves, their amplitudes and frequencies) depend on the P- and S-wave velocities, the bulk density and the thicknesses of the rock layer. The rate of change of elastic properties is related to the lithologic variation,

porosity, saturation of pore spaces, permeability, anisotropy, attenuation and pressure (Løseth *et al*., 2011). Determination of the relationship of these factors to the seismic response requires careful analysis and interpretation to indicate prospective zones in the vicinity of a well.

It is of crucial importance to use the seismic volume for the relative amplitude preservation (RAP) criteria to perform a lithofacies analysis (Cichostępski, 2016; Cichostępski *et al*., 2019). By fulfilling the above requirements, it is possible to determine the localization of sweet spots – the sites of relatively high kerogen content that can be potential exploration targets (Cichostępski and Kasperska, 2016).

The main aim of this project was to indicate sweet spots within the Lower Silurian deposits (Jantar Mudstone Formation) and Upper Ordovician (Sasino Mudstone Formation), which are considered to be potential shale gas exploration targets (Poprawa, 2010; Kiersnowski, 2013) A reservoir analysis was performed with the application of seismic inversion. The main problem was related to the insignificant thicknesses of the intervals analysed. The small thicknesses of both formations resulted in both signal interference and tuning that affected the seismic response. To overcome this

problem, the authors performed a resolution enhancement procedure (Kwietniak *et al.*, 2018), based on the blueing algorithm, and then proceeded with the seismic inversion. This paper is the English-language version of a chapter, previously published in a Polish monograph (Cichostępski *et al.*, 2017).

LOCATION OF STUDY AREA

The survey area is located within the inland part of the Baltic Basin. Two seismic datasets were used in the study (property of Polish Oil and Gas Company): the Kościerzyna-Gdańsk 2D survey (re-processed in 2009) and the Opalino 3D seismic survey (2013). Both surveys were processed with the RAP scheme. The data are of high quality and enabled seismic imaging up to the Proterozoic (depth of 5.1 km). The Kościerzyna-Gdańsk 2D seismic survey has a low signal-to-noise ratio beneath the Zechstein deposits, which is characteristic largely for the southern part of the survey with a predominant seismic wavelet of 25 Hz. The predominant seismic wavelet of the Opalino 3D seismic survey is 30 Hz.

For the analysis, well-log data from nine wells were used: O2, O3, O4, L1, Darżlubie-IG1, Ko1, Bo1, Wy1, and Kościerzyna-IG1. All these wells, except for the oldest, Darżlubie-IG1 and Kościerzyna-IG1, have complete well-log sets. The estimation of the kerogen content is missing from the oldest wells. The locations of the seismic data and the wells are shown in Figure 1.
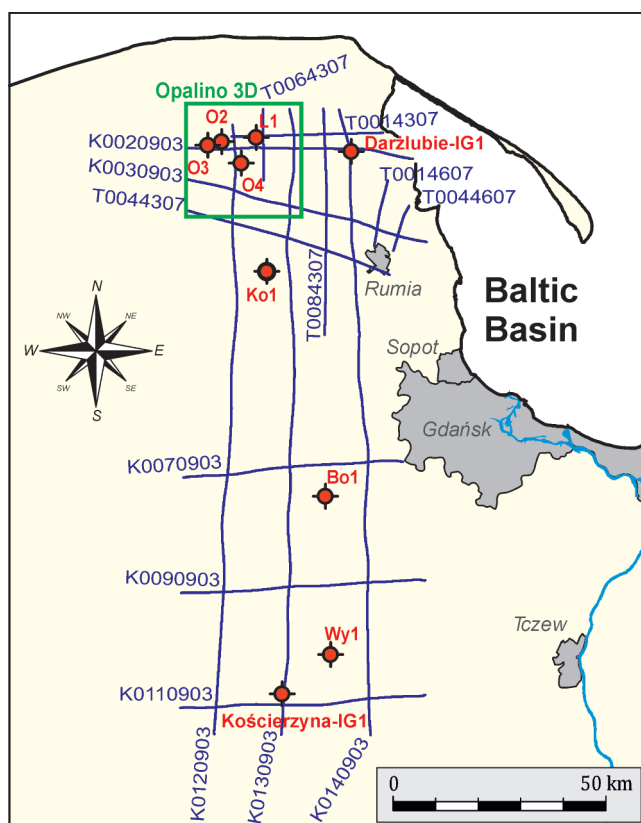
Fig. 1. Location of seismic surveys (blue lines – Kościerzyna-Gdańsk 2D, green rectangle – Opalino 3D seismic survey and wells (in red); after Cichostępski *et al.* (2017).

GEOLOGICAL INTERPRETATION OF SEISMIC DATA

Seismic-to-well tie

A seismic-to-well tie was performed with synthetic seismograms created for every available well in the study area. In this paper, the authors present a typical synthetic seismogram for well O3. For the synthetic seismograms, sonic profiling (DTP) was used, verified by means of checkshot measurements and density values (RHOB). The lithological information enabled computation of the acoustic impedance and reflectivity profiles (Fig. 2).

Well O3 is located within 3D, high-quality seismic data that are characterized by a good signal-to-noise ratio, which is crucial for wavelet extraction (Hampson and Galibraith, 1981). For the synthetic seismograms, the statistical wavelet was extracted from the seismic data in a time window between 1300-2400 ms. The seismic-to-well tie for the whole well is presented in Figure 2 and for the Lower Silurian and Ordovician deposits in Figure 6.

The high correlation coefficient of computed synthetic seismograms with seismic data enabled indication of the main lithostratigraphic units: J – top of the Jurassic, T – top of the Triassic, P – top of the Permian, S – top of the Silurian, Sb – top of the Reda Limestone Member, O – top of the Ordovician, Cm – top of the Cambrian. The top of the Proterozoic, which is not reached by well O3, was interpreted on the basis of information available from the vicinity of analysed 3D seismic data (wells Darżlubie-IG1 and Kościerzyna-IG1 as well as Kościerzyna-Gdańsk 2D seismic data).

Two more formations (Jantar and Sasino), characterized by increased organic matter content (VKER – kerogen volume), were also identified within the 3D seismic data (Fig. 6).

Structural interpretation

The seismic horizons, mentioned above, were recognized within the study area. Deposits of the Lower Palaeozoic, namely the Cambrian and the Devonian, are not present (stratigraphic gap). The Permian-Mesozoic strata were interpreted as a monocline, not much tectonically deformed, dipping towards the south (Figs 3–5).

Faults are present in the Lower Palaeozoic deposits mainly and do not continue into the Permo-Mesozoic interval. Faults in the southern part of the area are normal and homothetic with a NW-SE trend. The largest offset reaches 400 m (the Kościerzyna Fault). In the northern area, normal faults dominate, they have a NE-SW trend and sometimes of an anthythetic character. These faults were rejuvenated and inverted in the Late Silurian, when the stress regime changed to extensional. Such a hypothesis may be stipulated after careful analysis of the top of the Reda Member (Sb), which manifests itself in a different tectonic style compared to the older deposits. The top of the Reda Member includes many normal, thrust faults that are developed above the Proterozoic dislocations. The tectonic structure between the Ordovician (O) and the Reda Member (Sb) seismic horizons is not clear, which is most probably the result of the litholog-
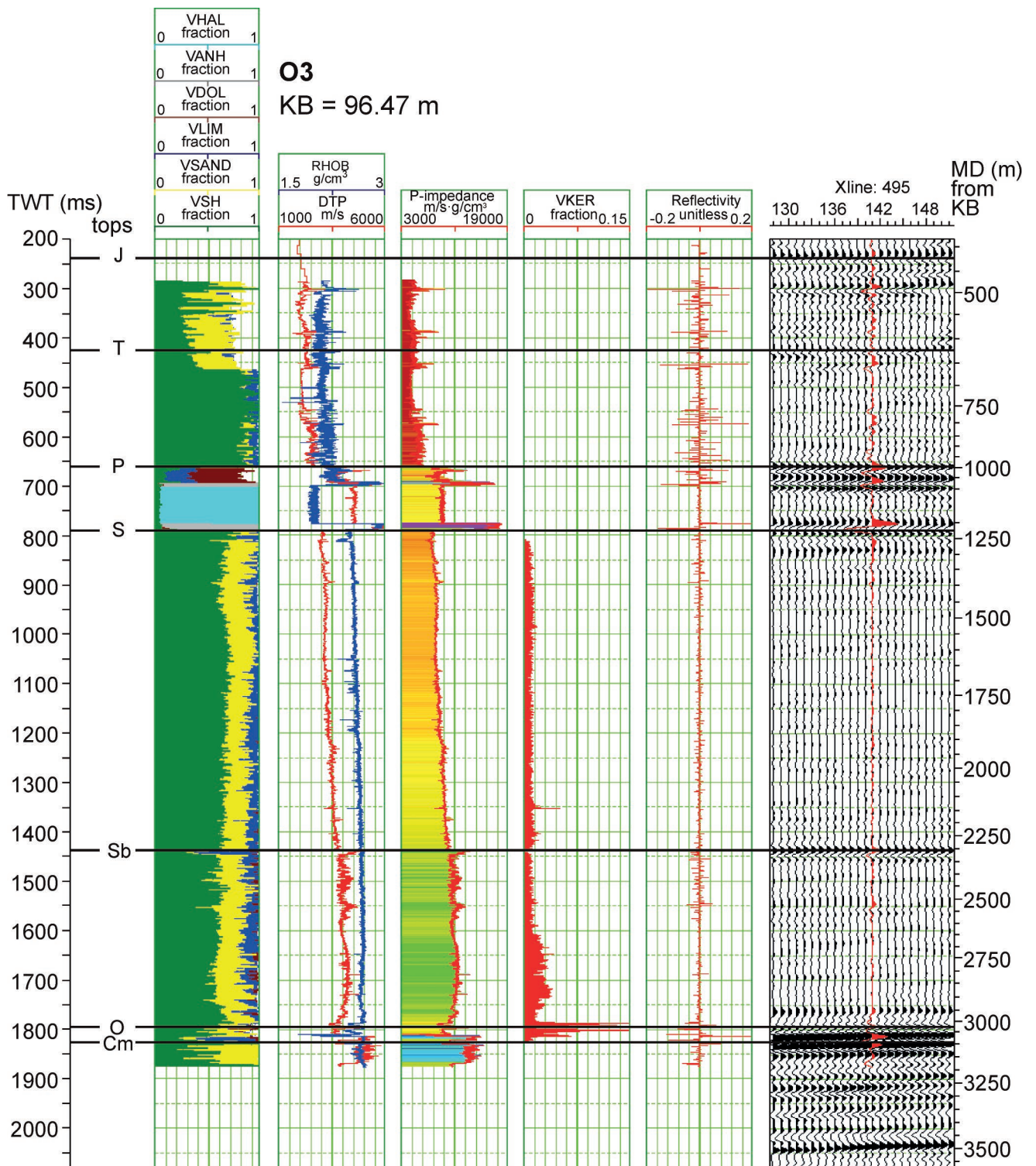
Fig. 2.   Well-to-seismic correlation at well O3. From left: lithology, P-wave velocity (DTP), bulk density (RHOB), P-impedance, kerogen volume (VKER), reflectivity, synthetic seismogram (in red) in comparison with the seismic data. J – top of Jurassic, T – top of Triassic, P – top of Permian, S – top of Silurian, Sb – top of the Reda Limestone Member, O – top of Ordovician, Cm – top of Cambrian; after Cichostępski *et al*. (2017).
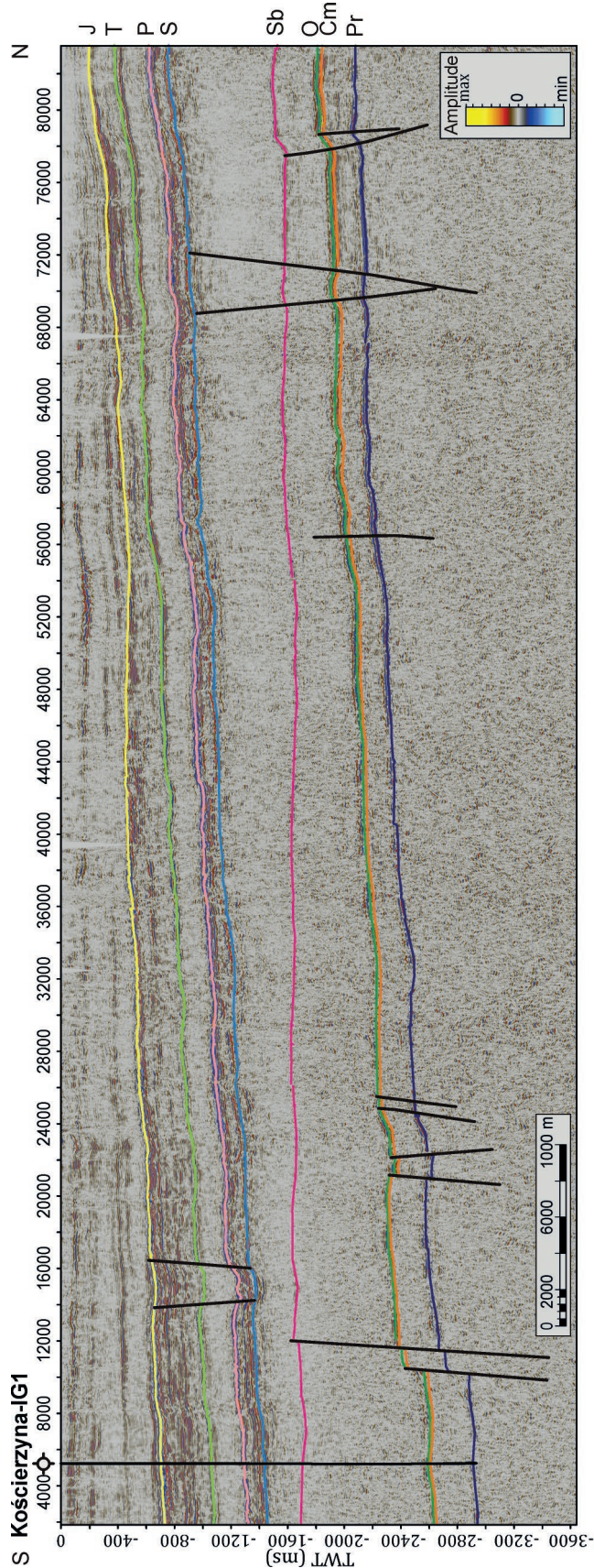
Fig. 3. Structural interpretation of K0130903 time profile. J – top of Jurassic, T – top of Triassic, P – top of Permian, S – top of Silurian, Sb – top of the Reda Limestone Member, O – top of Ordovician, Cm – top of Cambrian, Pre – top of Precambrian; after Cichostępski *et al.* (2017).

ical characteristics of these deposits, namely clay and mudstone heterolithies that have a ductile character.

The structural interpretation allowed the authors to conclude that (1) the late Palaeozoic (pre-Permian) erosion within the Baltic Basin reached the top parts of the Silurian deposits, and (2) the thickness distribution of the muddy-claystone complexes is linked mainly to the scale and the depositional environment in the basin, as well as to the location of the sediment source.

The tectonic disruption of the Lower Palaeozoic deposits within the Baltic Basin is relatively minor, which provides a favourable model for unconventional hydrocarbon accumulation and prospecting.

Organic matter content and its influence on the seismic signal parameters

The first step of the analysis was the comparison of the petrophysical parameters from wells with the seismic data from the vicinity of these wells. All wells available within the survey area show similar relationships and the typical results are illustrated for well O3. The interval of interest is the Lower Silurian and Ordovician and the analysis was limited to this interval exclusively.

The lowermost Silurian strata are referable to the Jantar Mudstone Formation. Thicknesses are within the range of 12–15 m. The average kerogen content here is 6%, reaching a maximum of 16% (well O4). The Jantar Formation rests on limy-marly Ordovician sediments; lower in the profile is the Sasino Formation, composed of black claystones. The prospective Sasino Formation has thicknesses of between 16 m (well Bo1) and 25 m (well L1). The average kerogen content is 6%, reaching a maximum value of 17% (well Ko1). Organic matter is present mainly in the uppermost part of the Sasino Formation.

The increase in the organic matter content results in the decrease of the seismic wave velocity (DTP) and bulk density (RHOB), which in turn gives a decrease in acoustic impedance. Both perspective formations are underlain by deposits that have higher acoustic impedances (marls of the Prabuty Formation and limestones of the Kopalino Formation). Such a relationship between petrophysical parameters results in the tops of both perspective formations having negative seismic reflections (negative reflection coefficients), while their beds display positive seismic reflections. For the analysed reflections, these differences are lower for the Jantar Formation and higher for the Sasino Formation, which is related to the amplitude of the seismic reflections produced.

RESERVOIR CHARACTERIZATION WITH ACOUSTIC IMPEDANCE

The seismic inversion process can provide information about the petrophysical properties of deep deposits (Kasina, 1998). This method utilizes seismic and well data to transform the seismic data from the reflectivity domain to the impedance domain. Analysing the data in the impedance domain enables its detailed interpretation (Latimer *et al.*, 2000;
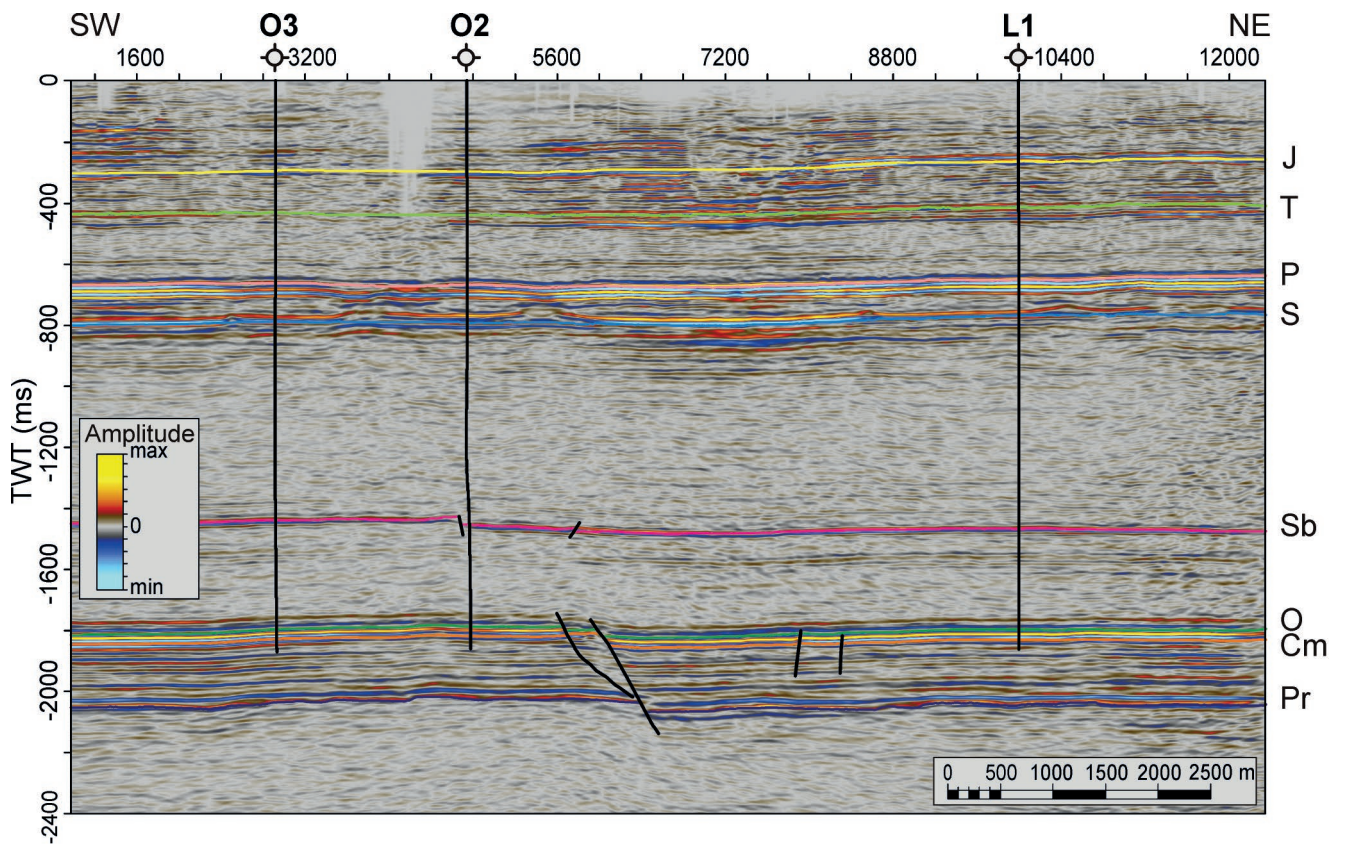
Fig. 4. Structural interpretation of an arbitrary section through wells O3-L1 (Opalino 3D seismic survey). J – top of Jurassic, T – top of Triassic, P – top of Permian, S – top of Silurian, Sb – top of the Reda Limestone Member, O – top of Ordovician, Cm – top of Cambrian, Pre – top of Precambrian; after Cichostępski *et al.* (2017).
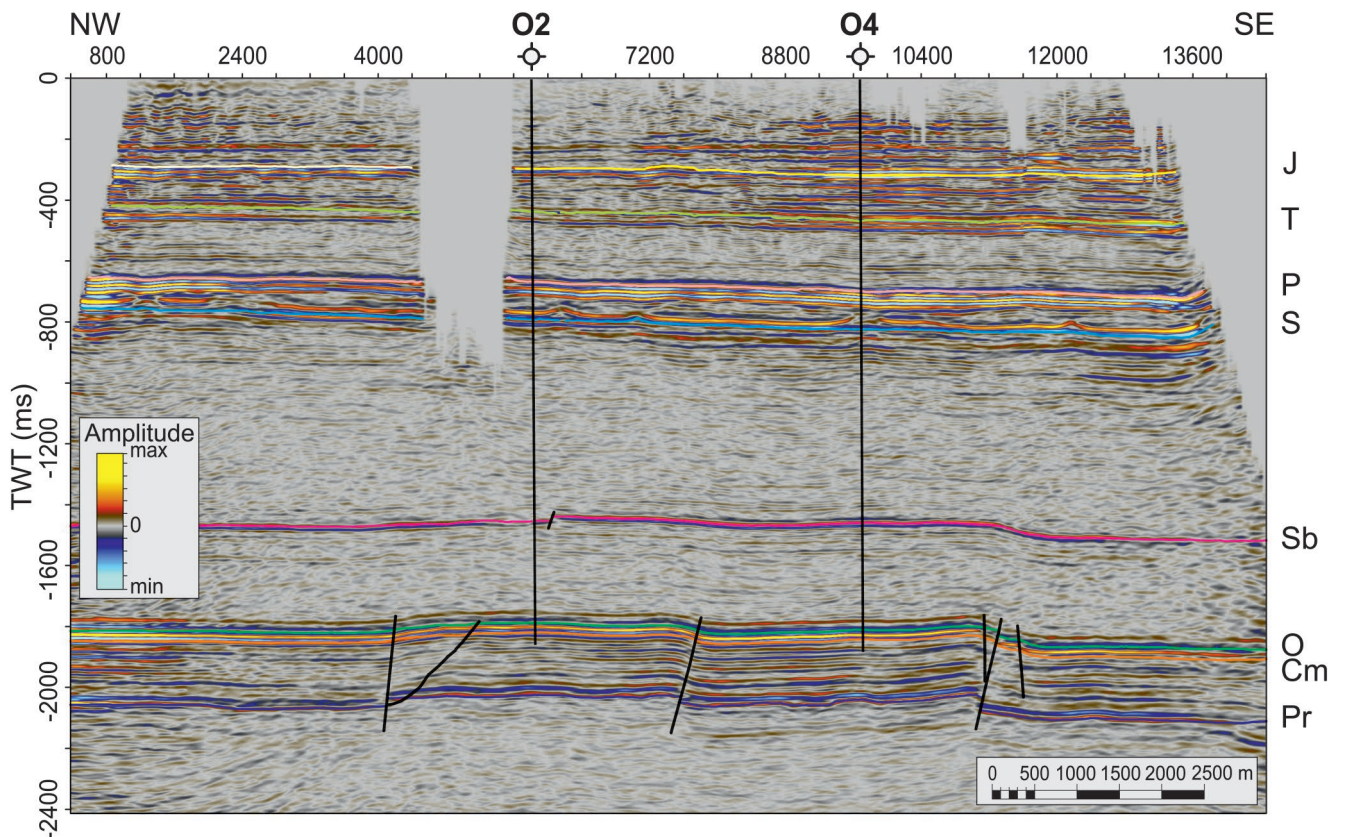
Fig. 5. Structural interpretation of an arbitrary section through wells O2-O4 (Opalino 3D seismic survey). J – top of Jurassic, T – top of Triassic, P – top of Permian, S – top of Silurian, Sb – top of the Reda Limestone Member, O – top of Ordovician, Cm – top of Cambrian, Pre – top of Precambrian; after Cichostępski *et al.* (2017).
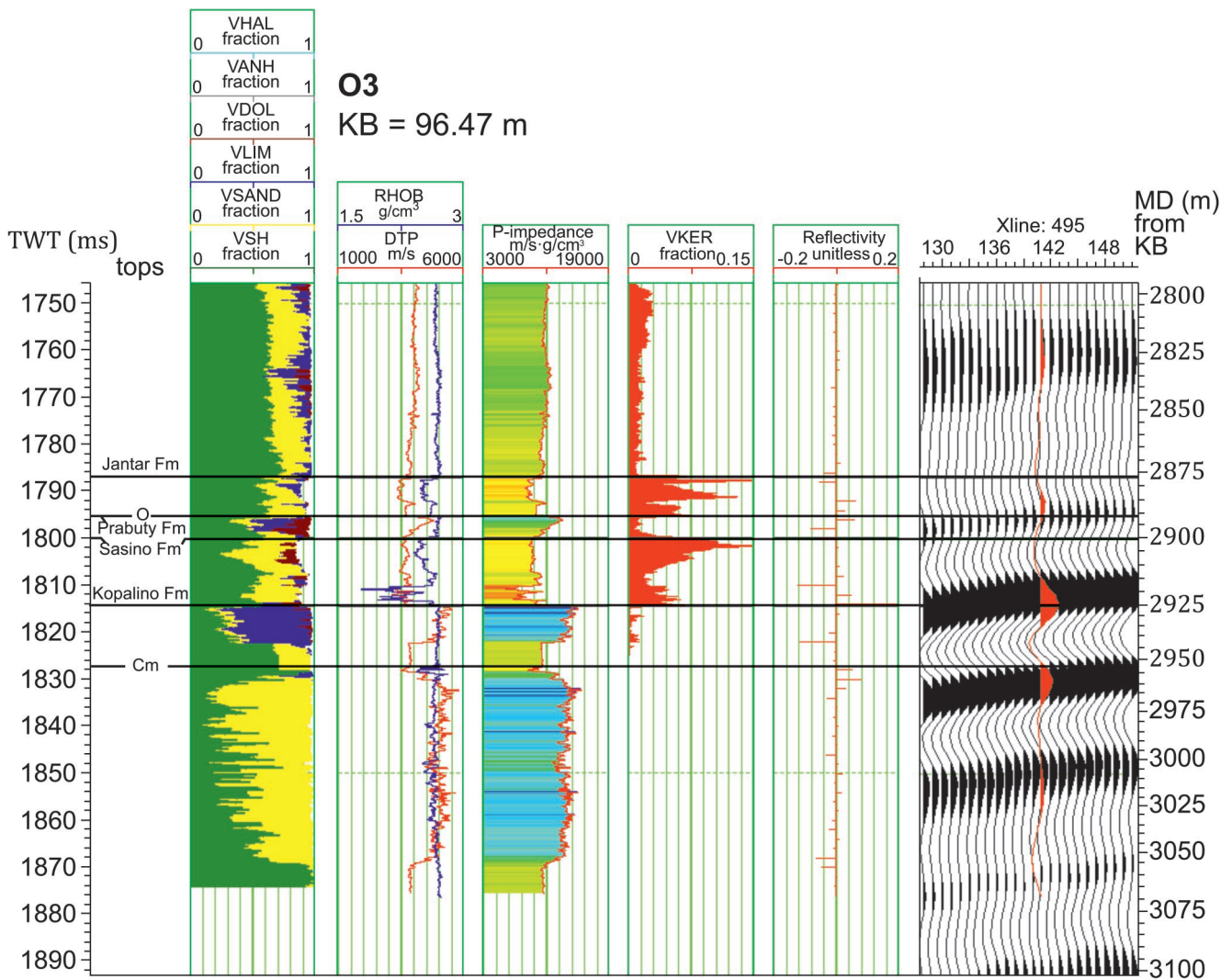
Fig. 6. Well-to-seismic correlation for Lower Palaeozoic deposits at well O3. From left: lithology, P-wave velocity (DTP), bulk density (RHOB), P-impedance, kerogen volume (VKER), reflectivity, synthetic seismogram (in red) in comparison with the seismic data. O – top of Ordovician, Cm – top of Cambrian; after Cichostępski *et al.* (2017).

Pendrel, 2006). The variation in acoustic impedance can be related to lithological and porosity changes, gas saturation or the presence of organic matter. An increase in kerogen content causes a drop in seismic velocity and density, which results in a decrease in acoustic impedance. Such zones are interesting from the point of view of hydrocarbon prospecting and can be potential exploration sites.

Acoustic impedance in relation to kerogen content

Before proceeding with the inversion process, as a first step the authors examined types of relationship between acoustic impedance values and the kerogen content for the two prospective intervals, the Sasino and Jantar formations. The results of these analyses are shown as cross-plots (Figs 7–13). An additional parameter that is depicted by these plots is the effective porosity.

For the Jantar Formation, a non-linear relationship between the acoustic impedance and the kerogen content can be observed. The lowest impedance values are associated with relatively high porosity values (3–7%) and a kerogen content of about 6–7%. These values can be classified as the most prospective for the Jantar Formation. An increase in the kerogen content results in a lowering of the porosity and does not produce further changes in acoustic impedance.

The Sasino Formation has a higher quartz content by comparison with the muddier Jantar Formation. Similarly, the nature of the relationship between kerogen content and acoustic impedance is non-linear. The most abrupt drops in acoustic impedance are linked to sandstone intercalations with high porosity (8–10%), for which the kerogen content reaches up to 4%. Higher values of kerogen content were obtained for the more illitic deposits. In this case, a further decrease in acoustic impedance is related to kerogen content of 4% and average porosity values of between 3–4%. A further increase in the kerogen content causes a decrease in of the porosity but does not affect the acoustic impedance changes. In well O4 (Fig. 9), sandy intercalations are present in the interval analysed and have a porosity of 18%, with a kerogen content of 8%. In the illitic (claystone) packets, the kerogen content reaches a maximum of 28%. This value,
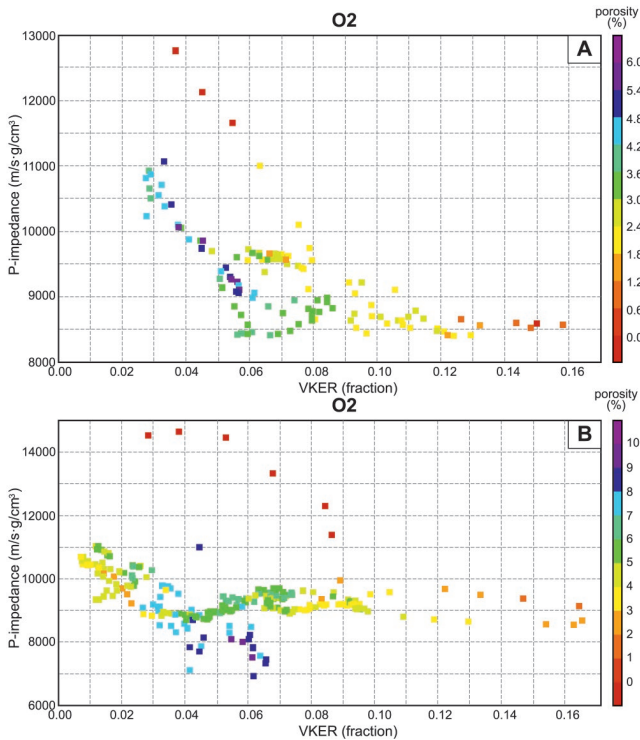
Fig. 7.   Relationship between acoustic impedance (P-impedance) and kerogen volume (VKER) for well O2, porosity in colour. **A.** Jantar Formation. **B.** Sasino Formation; after Cichostępski *et al*. (2017).
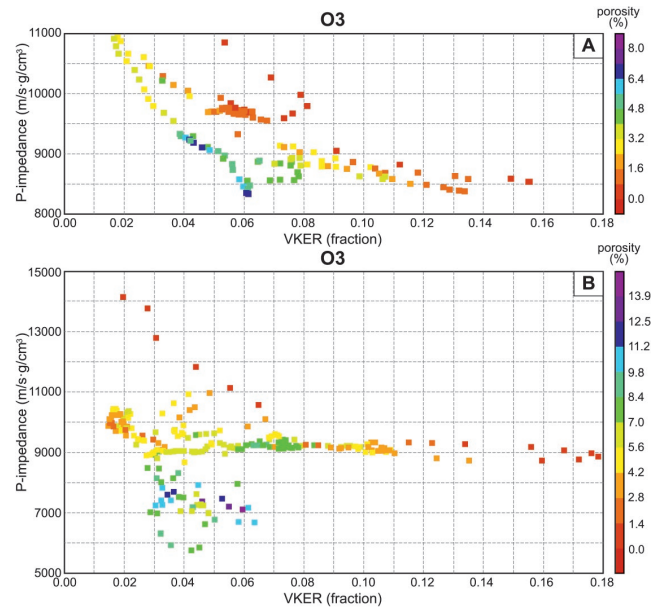
Fig. 8.   Relationship between acoustic impedance (P-impedance) and kerogen volume (VKER) for well O3, porosity in colour. **A.** Jantar Formation. **B.** Sasino Formation; after Cichostępski *et al*. (2017).
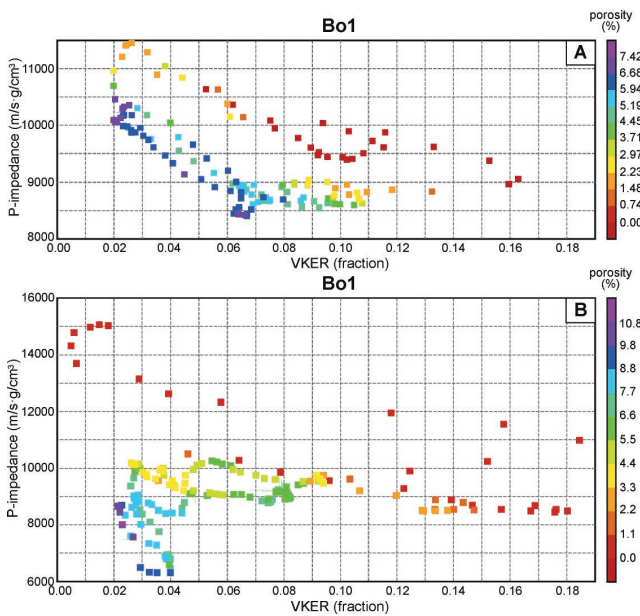
Fig. 9.   Relationship between acoustic impedance (P-impedance) and kerogen volume (VKER) for well O4, porosity in colour. **A.** Jantar Formation. **B.** Sasino Formation; after Cichostępski *et al*. (2017).
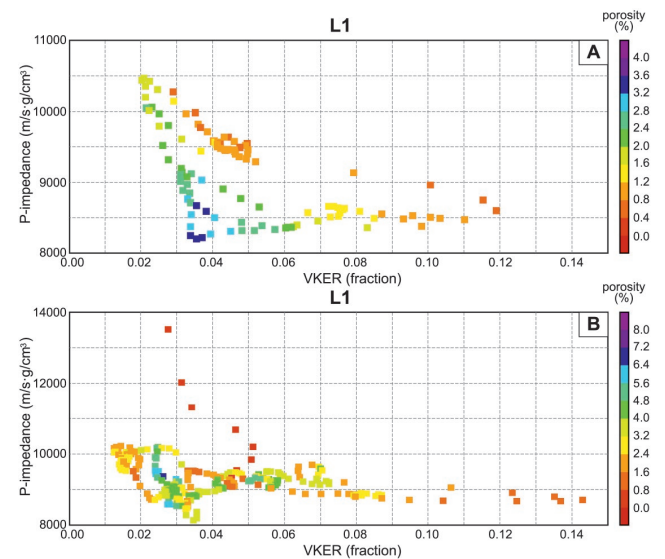
Fig. 10.   Relationship between acoustic impedance (P-impedance) and kerogen volume (VKER) for well L1, porosity in colour. **A.** Jantar Formation. **B.** Sasino Formation; after Cichostępski *et al*. (2017).
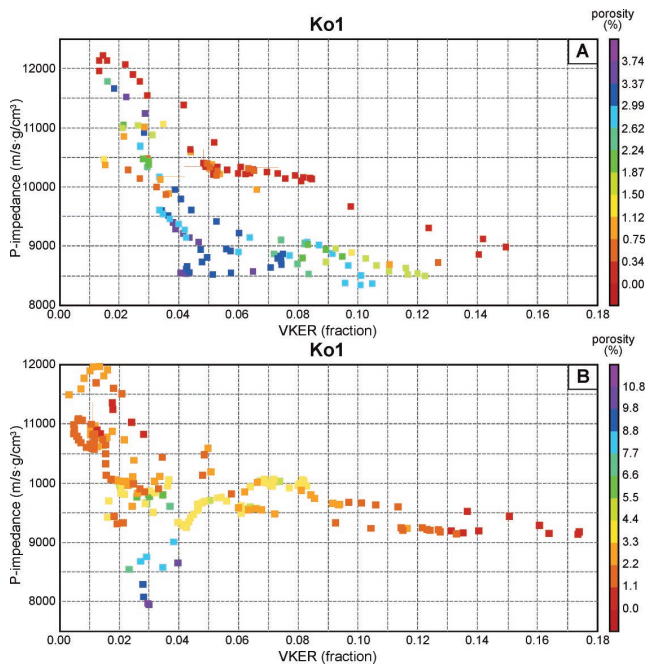
Fig. 11. Relationship between acoustic impedance (P-impedance) and kerogen volume (VKER) for well Ko1, porosity in colour. **A.** Jantar Formation. **B.** Sasino Formation; after Cichostępski *et al.* (2017).
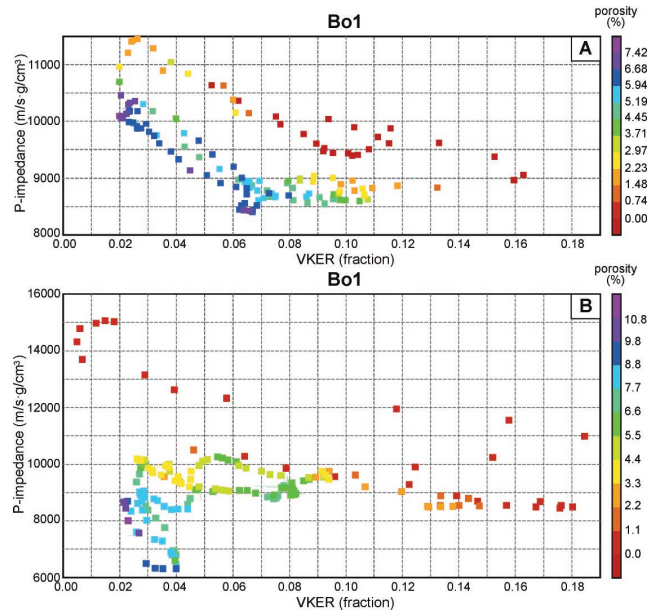
Fig. 12. Relationship between acoustic impedance (P-impedance) and kerogen volume (VKER) for well Bo1, porosity in colour. **A.** Jantar Formation. **B.** Sasino Formation; after Cichostępski *et al.* (2017).
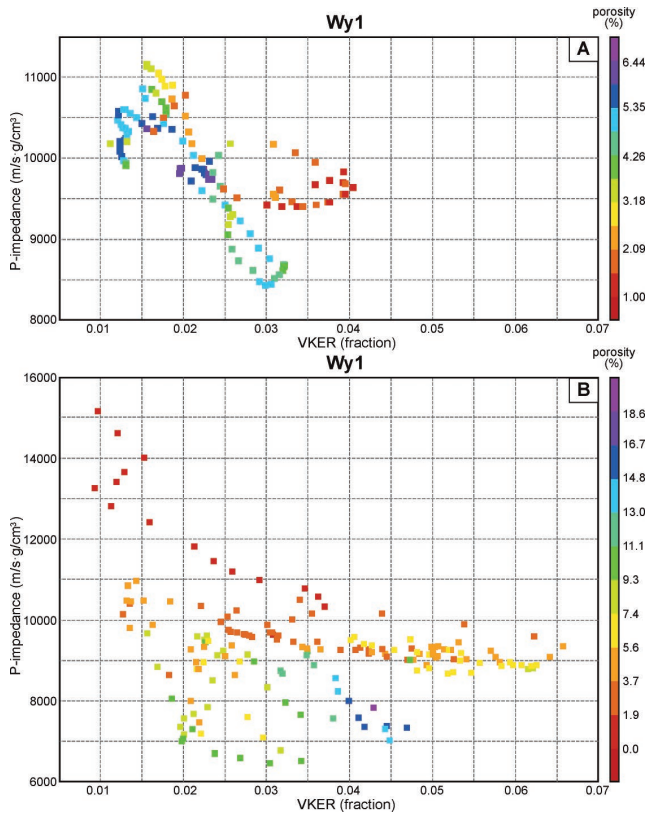
Fig. 13. Relationship between acoustic impedance (P-impedance) and kerogen volume (VKER) for well Wy1, porosity in colour. **A.** Jantar Formation. **B.** Sasino Formation; after Cichostępski *et al.* (2017).

however, does not seem to be valid and most probably is the result of incorrect interpretation.

The increase in kerogen content results in a non-linear decrease of acoustic impedance (P-impedance) for both the Jantar and Sasino formations. Therefore, the most prospective sites should be linked to the lowest acoustic impedance values.

METHODOLOGY FOR THE INVERSION PROCESS

The process of inversion is based on the deconvolution model of a seismic trace, in which the seismic trace is defined by

$$S(t) = W(t)*R(t) + N(t)$$

where
s(t) – complex seismic trace,
W(t) – source wavelet,
R(t) – reflectivity function in a time domain,
N(t) – additive noise.

The reflectivity function is defined as an impedance contrast (P-wave impedance) between two geological layers:

$$r_{Pi} = \frac{\rho_{i+1} V_{Pi+1} - \rho_i V_{Pi}}{\rho_{i+1} V_{Pi+1} + \rho_i V_{Pi}} = \frac{Z_{Pi+1} - \rho_i V_{Pi}}{Z_{Pi+1} + Z_P}$$

where
r_{pi} – reflection coefficient for the normal incident angle of a seismic wave on the i-th seismic boundary
ρ – bulk density,
V_P – P-wave velocity,
Z_{Pi} – P-impedance.

The source wavelet that is required for the inversion process is extracted from the seismic data S(t). Such estimation is used in the deconvolution process that brings the seismic trace S(t) to the reflectivity function. The P-impedance then is computed recursively on the basis of the relationship given by Lindseth (1979) in the form:

For the calculation of impedance P, a Post-Stack Model-Based Inversion was used (Veeken and Da Silva, 2004; Russell, 1988). In this method, a simple low-frequency model of the Earth's geology is designed through the interpolation of well-log measurements (sonic and bulk density) along interpreted horizons and then recursively altered, until the derived synthetic section best fits the original seismic data.

The initial model was created on the basis of logs from the O2, O3, L1, Ko1, Bo1 and Wy1 wells. For computations, the statistical signal extracted from the seismic data between the top of the Reda Limestone Member (Sb) and the top of Proterozoic (Pr) was used. The inversion process was performed in the time window between 300 and 4000 ms.

RESULTS

Figure 14 shows the distribution of the acoustic impedance along the seismic profile K0020903 from the Kościerzyna-Gdańsk 2D seismic survey and the corresponding profile from the Opalino 3D seismic survey. By the comparison of these two, it may be concluded that owing to the poor quality of 2D seismic data, the results of seismic inversion are very poor and cannot be used for prospect-related reasoning.

The results obtained for 3D seismic data (Fig. 14B) show the layer of decreased acoustic impedance (just above the Cm seismic horizon). This layer corresponds to an increased value of the kerogen content. Such a layer is visible in the whole 3D seismic survey.

The localization of prospective sites within the Opalino 3D seismic data

Figure 15 shows part of seismic profile between wells O3-L1 and Figure 16 between wells O2-O4. These profiles are combined with the inversion results. The curve visible here is the volumetric kerogen content (VKER). In both profiles, the Jantar Formation and the Sasino Formation manifest themselves with low values of acoustic impedance, which also corresponds to the increased value of the kerogen content estimated from the well logs. The layer of the Jantar Formation is underlain by the very thin Prabuty Formation, which is also the top of the Ordovician sequence. Below lies the Sasino Formation, which is underlain by the high-impedance, limy Kopalino Forma-
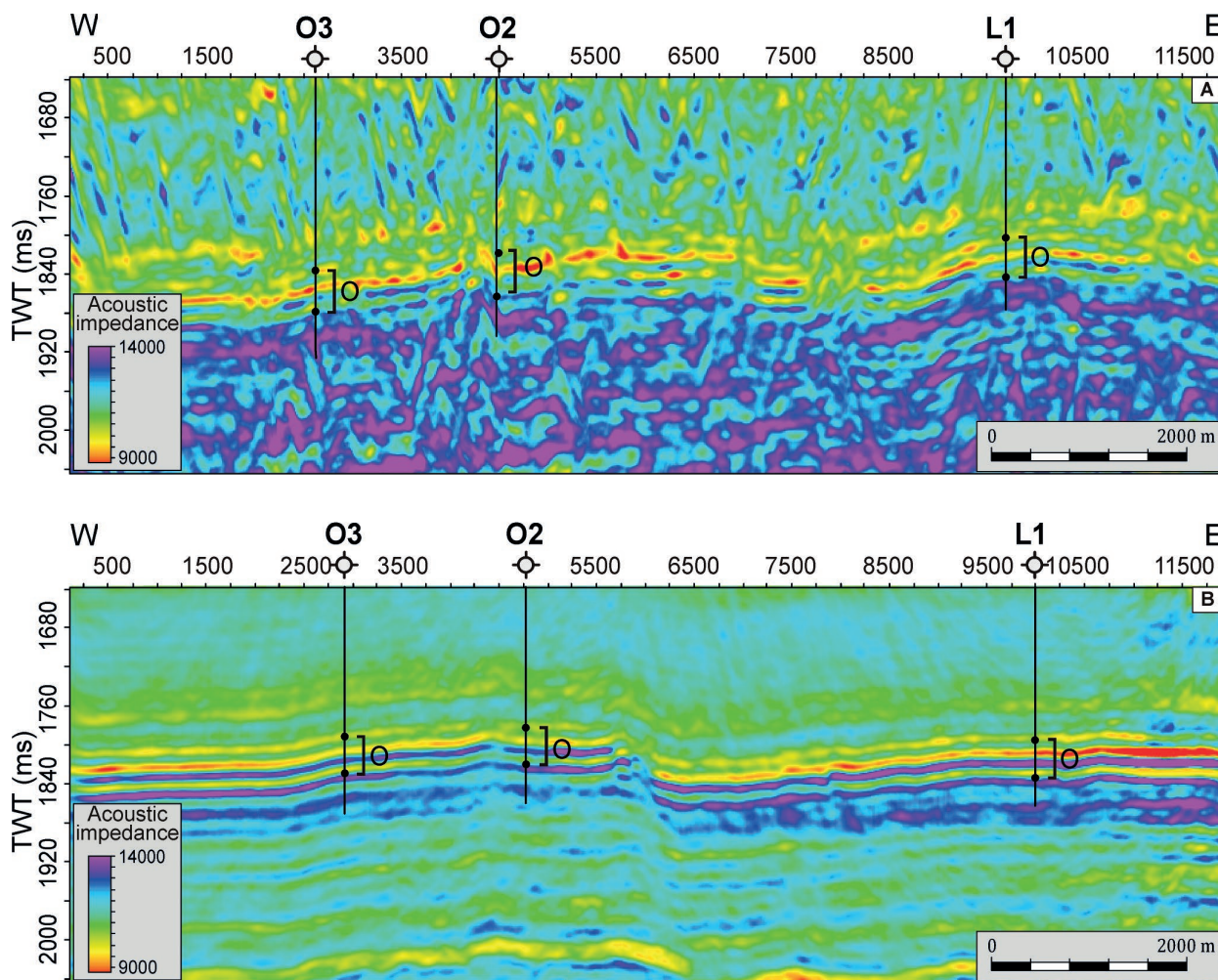
Fig. 14. Acoustic impedance volumes. **A.** Profile K0020903 from 2D seismic survey. **B.** Corresponding profile from 3D seismic survey. O – Ordovician; after Cichostępski *et al.* (2017).
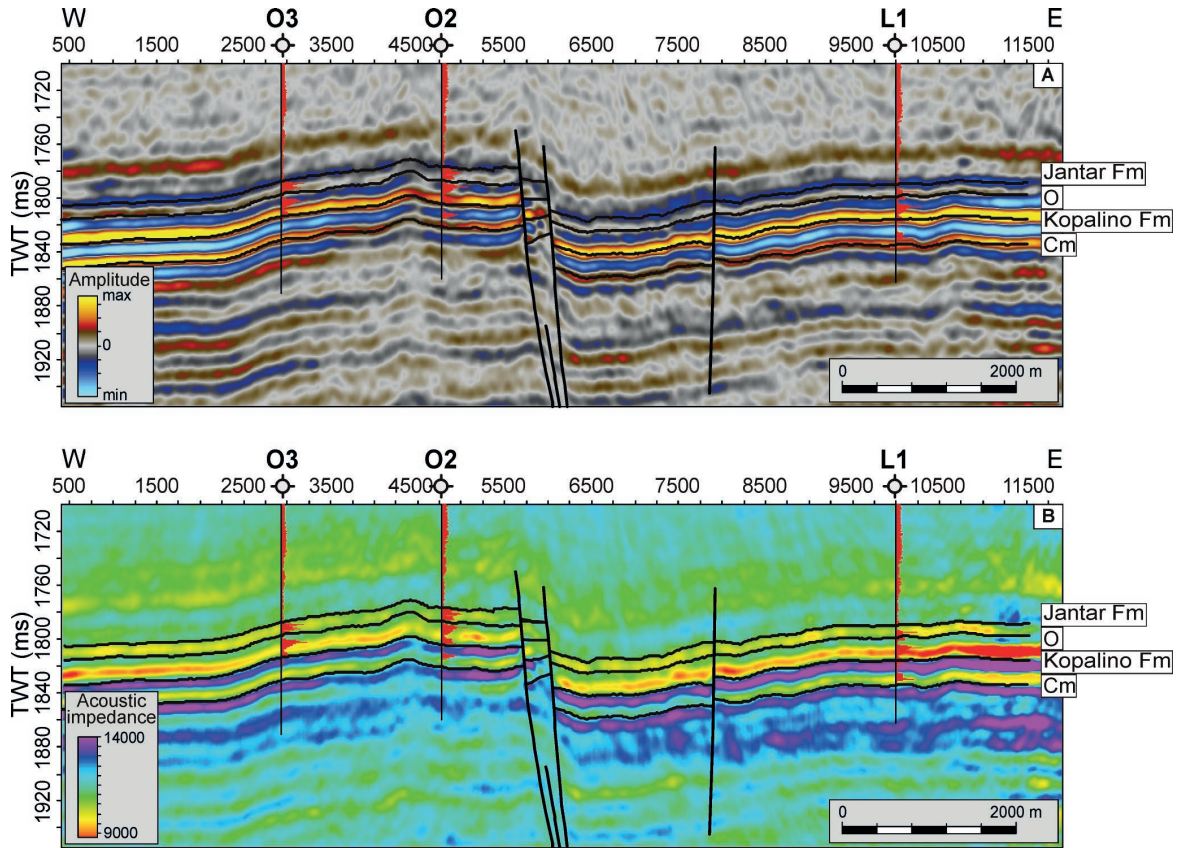
Fig. 15. Seismic and acoustic inversion between wells O3-L1. **A.** Part of an arbitrary seismic profile. **B.** Results of acoustic inversion in the same profile. Well data: VKER. O – top of Ordovician, Cm – top of Cambrian; after Cichostępski *et al.* (2017).
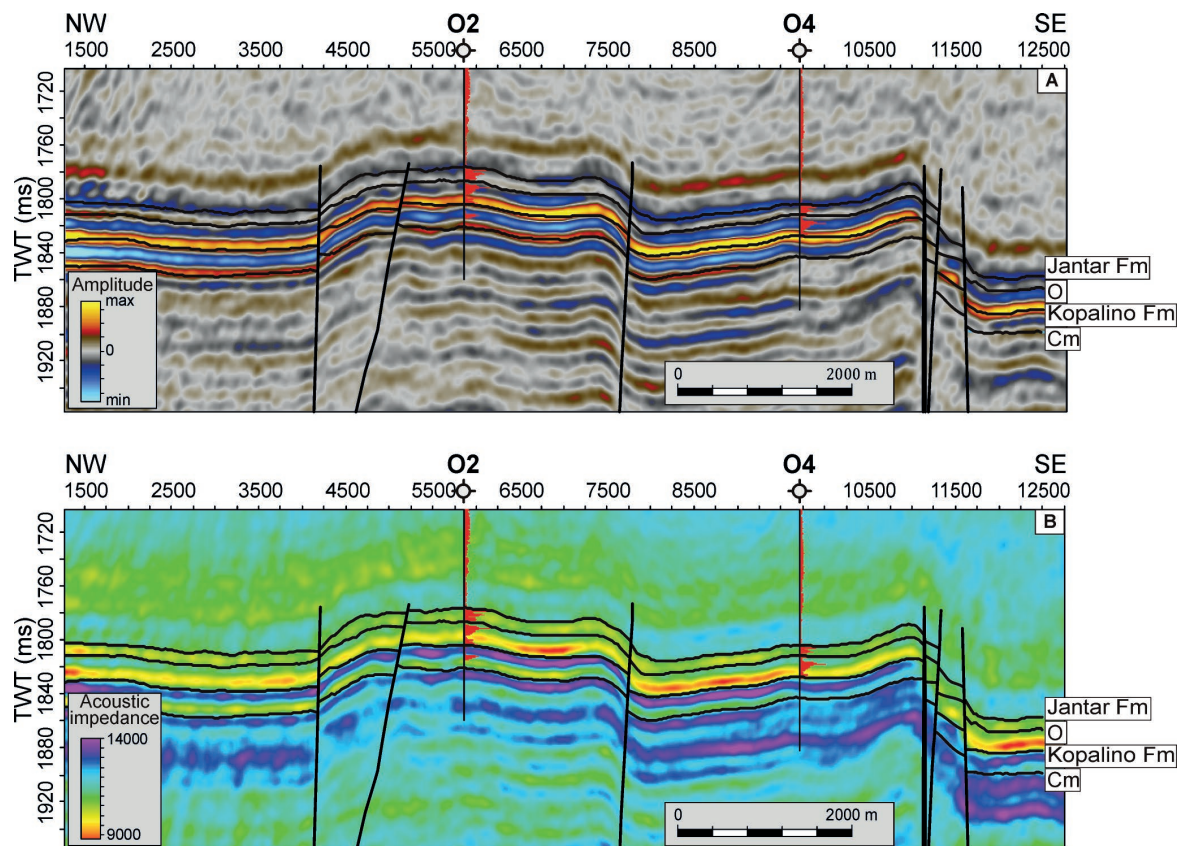
Fig. 16. Seismic and acoustic inversion profile between wells O2-O4. **A.** Part of the arbitrary seismic profile. **B.** Results of acoustic inversion in the same profile. Well data: VKER. O – top of Ordovician, Cm – top of Cambrian; after Cichostępski *et al.* (2017).

tion. The Sasino Formation is characterised by a more diverse distribution of organic matter. This formation also yields the lowest impedance values. The average acoustic impedance value for the Jantar Formation (Fig. 17) reaches 10500 m/s*g/cm^3, while for the Sasino Formation it is 9600 m/s*g/cm^3 (Fig. 18). The most rapid decrease in acoustic impedance (9900 m/s*g/cm^3 for the Jantar Fm and 8600 m/s*g/cm^3 for the Sasino Fm) corresponds mainly to the lowermost morphological positions (opposite to conventional targets). The results indicate that the zones with the lowest impedance values may be related to the areas of higher organic matter content.

The spatial distribution of the acoustic impedance values for the Jantar Formation is presented in Figure 17; for the Sasino Fm a corresponding map is shown in Figure 18. In the case of the Jantar Formation, the zones of the lowest acoustic impedance values lie on both the hanging wall and footwall of the SW-NE fault zone. In the case of the hanging wall, the most promising zone corresponds to the values of 9600 m/s*g/cm^3 in the central part of the 3D seismic survey. Within the footwall, the most prominent zone lies within its southern part. The acoustic impedance values here reach 9200 m/s*g/cm^3.
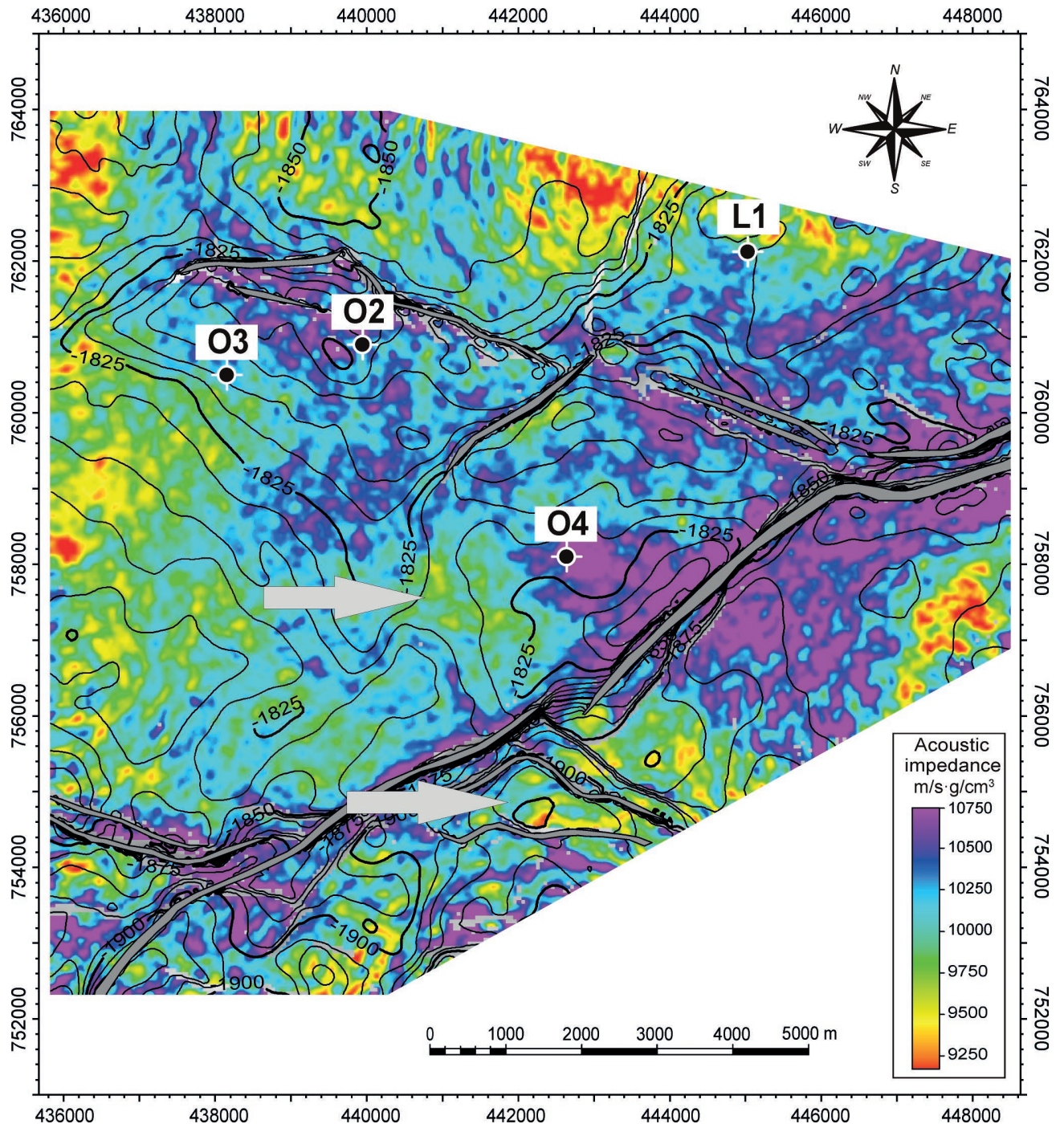
Fig. 17. The spatial distribution of acoustic impedance versus the structural time map for the Jantar Formation. Arrows indicate potential sweet spots; after Cichostępski *et al.* (2017).
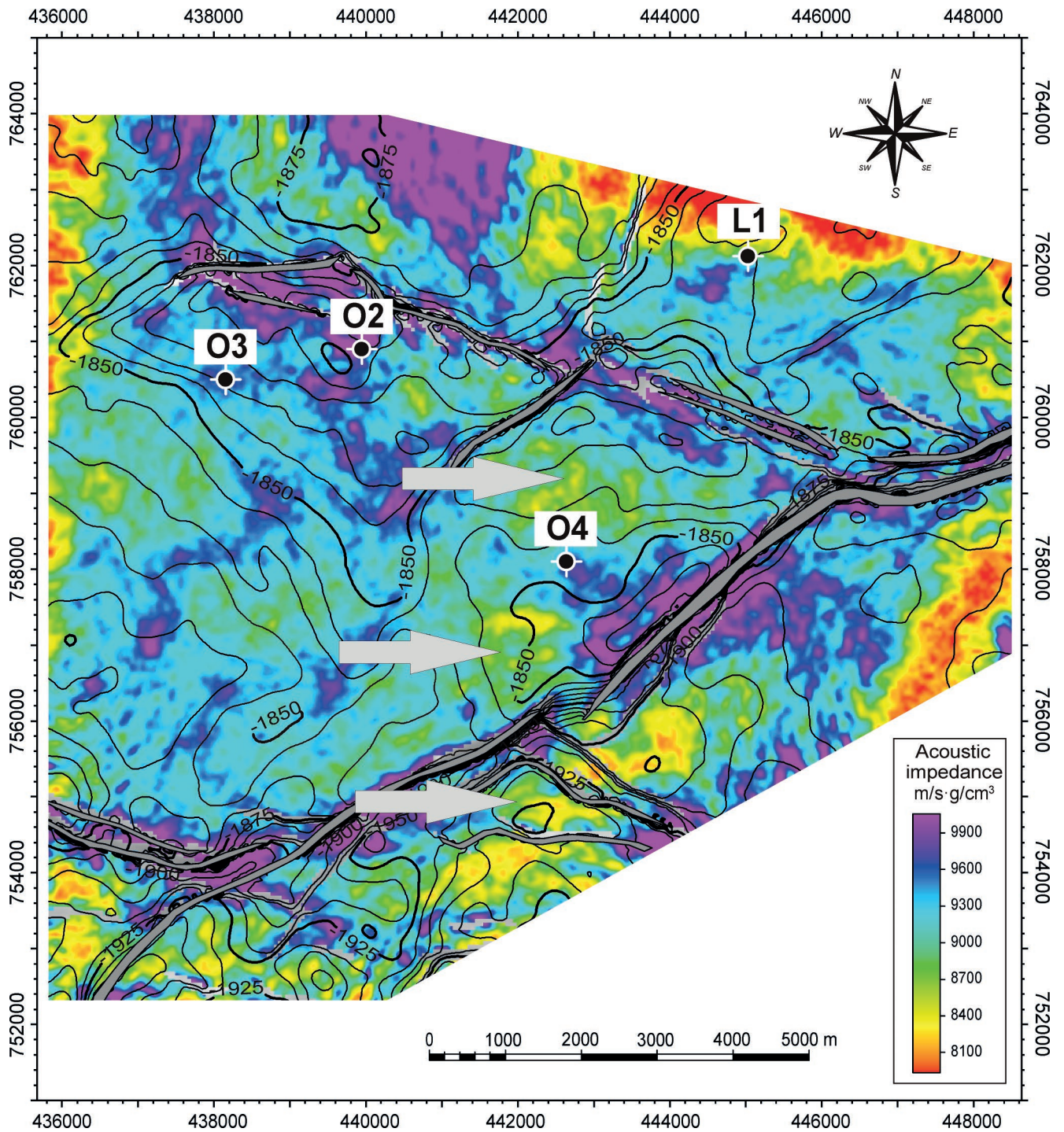
Fig. 18. The spatial distribution of acoustic impedance versus the structural time map for the Sasino Formation. Arrows indicate potential sweet spots; after Cichostępski *et al*. (2017).

A similar situation can be observed in the Sasino Formation. In this case, the lowest zones of acoustic impedance are related to the faulting zone with a SW-NE direction. For the Sasino Formation, the decrease in the acoustic impedance is higher (from 8600 to 8100 m/s*g/cm³). These zones are indicated in Figures 17 and 18 by arrows and can be designated as potential exploration sites. Zones of decrease in acoustic impedance that are present along the borders of the 3D seismic data are the result of decreased

fold and should be excluded from considerations of reservoir occurrence.

Interpretation of thin bed setting and resolution enhancement

The lower Silurian and Ordovician deposits can be considered as thin-bedded intervals (Widess, 1972; Zeng, 2015). This characteristic significantly complicates and sometimes

even invalidates the interpretation process. A method that can enhance the resolution of seismic data that is based on convolution is called spectral blueing. This concept uses the assumption that for interpretation of seismic data, blue reflectivity is preferable (Walden and Hosken, 1985).

The reflectivity of a seismic section can be characterised as a function of a long and complicated impulse response. On the basis of the power spectra of such functions, the signals have nomenclature related to the colours of the light (Walden and Hosken, 1985). The white spectrum, in an analogue to visible light, is a spectrum that has the constant energy for all frequency components. Signals of the red spectrum show higher energies for lower and blue for higher frequencies. Blue reflectivity is characteristic for geological sequences that consist of several thick layers and many thin layers.

Many resolution-enhancing methods assume that the Earth's reflectivity should have white characteristics. The conventional seismic whitening (based, for example, on spike deconvolution) modifies the signal, which in consequence often decreases the resolution. The spectral blueing procedure, however, uses the paradigm that the Earth's reflectivity should have a blue character and the algorithm aims to recover blue reflectivity of seismic data. This effect is obtained by applying a blueing operator, which is constructed from well data. To create the operator, the reflectivity function is recovered, on the basis of velocity and density profiling. The spectrum of the reflectivity series produced from well data is then compared with the spectrum of seismic data. This comparison enables the creation of a blueing operator that can be applied to seismic data in a convolution process. This method is especially effective in a thin bed setting, where signal interference results in a tuning effect (Kwietniak *et al.*, 2018).

This procedure was applied to seismic data to enable more precise structural interpretation and a more accurate inversion process.

Comparison of inversion results performed after spectral blueing

After the application of the spectral blueing procedure, the authors proceeded with the second inversion procedure. All the parameters were kept the same, except for a new, statistical wavelet that was extracted from the seismic data after spectral blueing. The comparison of two inversions for an arbitrary seismic profile is shown: without resolution enhancement and after spectral blueing for profiles O3-L1 (Fig. 19) and profile O2-O4 (Fig. 20).

The distribution of acoustic impedance did not change after the application of spectral blueing. What did change was the range of the impedance values, which widened. For the Jantar Formation, the spatial distribution of low impedance anomalies was not modulated (Fig. 21), but the values are lower at 100–300 m/s*g/cm^3. In the case of the distribution of low impedance anomalies for the Sasino Formation, two more potential exploration sites are more clear (red arrows in Fig. 22).

SUMMARY AND CONCLUSIONS

The focal part of this analysis was to indicate potential shale gas exploration sites within the Lower Silurian (Jantar Formation) and Upper Ordovician (Sasino Formation). The identification of these areas (sweet spots) was possible with the use of the high-quality seismic and well data from the wells that are localized within the survey area. The preliminary steps enabled the authors to state that a non-linear relationship exists between the kerogen content and acoustic impedance for both prospecting formations. The well data on their own, however, cannot be used to localize the positions of potential exploration sites within the study area. It is possible to indicate them only with the use of acoustic inversion, computed for the entire seismic volume. 3D seismic data are necessary for this process, as the 2D data are not adequate for performance of a lithofacies analysis. The results of acoustic impedance can be used for prospecting purposes.

The relative thicknesses of the analysed interval impact on the seismic signature of the Lower Silurian and Upper Ordovician deposits and influence the results of the inversion process. To overcome this effect by enhancing the resolution of seismic data, the authors performed the spectral blueing procedure and then proceeded with the inversion process on the enhanced seismic data. With the use of the latter, it was possible to determine two more potential exploration sites for the Sasino Formation.

The spectral blueing procedure was an effective tool in the analysis, which the authors value highly for the resolution enhancement algorithm.

The distribution of the acoustic inversion performed with the use of P-wave velocity can only give information that is valid for a zero-offset scenario, i.e. for the normal incident angle. In this approach, changes of amplitudes with offsets/angle (caused by Poisson ratio changes and Vp/Vs variations) are not considered (Cichostępski, 2016). To consider these factors, a simultaneous inversion is required (Hampson *et al.*, 2005). It is strongly recommended that shear velocity profiling be routinely performed; this would result in obtaining the logs necessary for simultaneous inversion. Availability of both P- and S-impedances would be also essential for computing other geomechanical parameters, such as $\lambda\rho$, $\mu\rho$, Vp/Vs (Goodway *et al.*, 1997, 2010; Cichostępski and Kasperska, 2016), Poisson ratio and Young modulus (Gray *et al.,* 2012). The information provided by these geomechanical factors is of paramount importance for hydraulic fracturing. For simultaneous inversion, high-quality pre-stack data with preserved relative amplitudes and shear wave velocity profiling are required.

Another type of data that would be of great help would be VSP (vertical seismic profiling) data in all configurations (zero-offset, offset, 3D and walk-away). Such data would give an immediate link between well logs and seismic data. VSP data also provide information about multiples that can be used in seismic data processing and might give some information about attenuation phenomena, anisotropy and AVO.
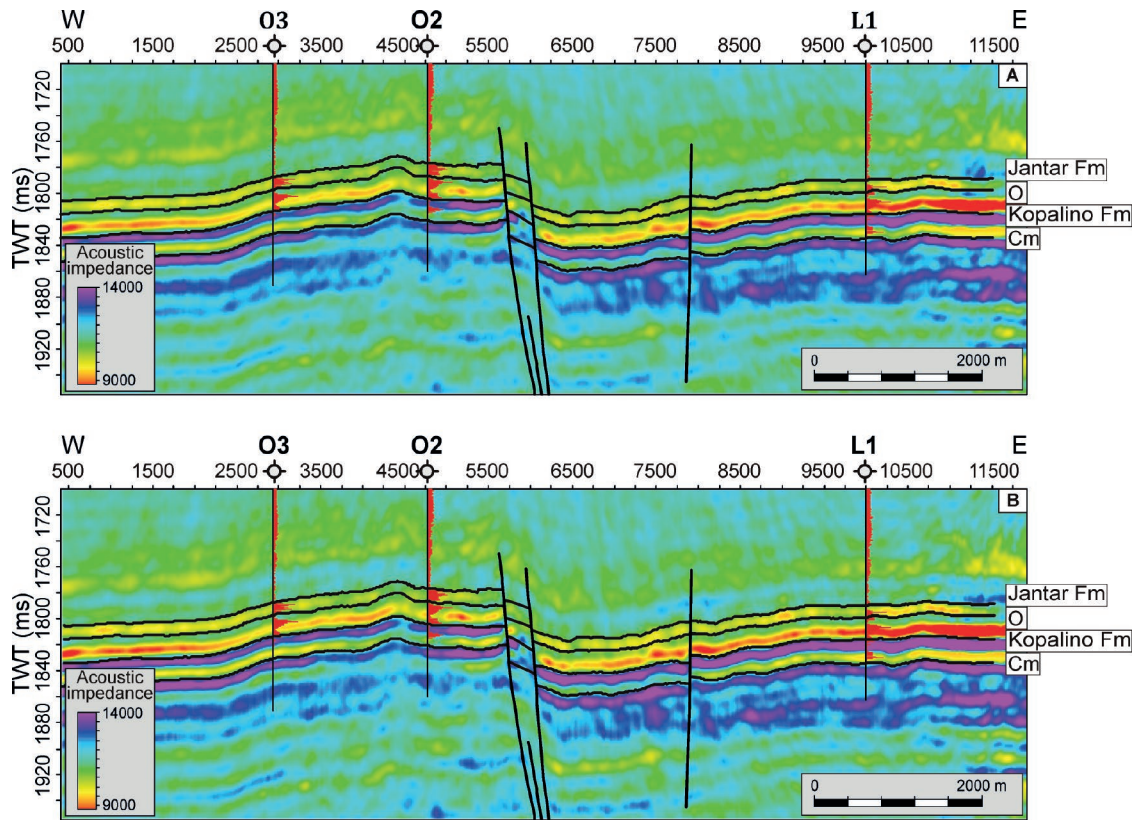
Fig. 19. Segment of an arbitrary seismic profile between wells O3-L1 after acoustic inversion. **A.** Original seismic data. **B.** After resolution enhancement with spectral blueing. Well data: VKER. Arrows indicate potential sweet spots. O – top of Ordovician, Cm – top of Cambrian; after Cichostępski *et al*. (2017).
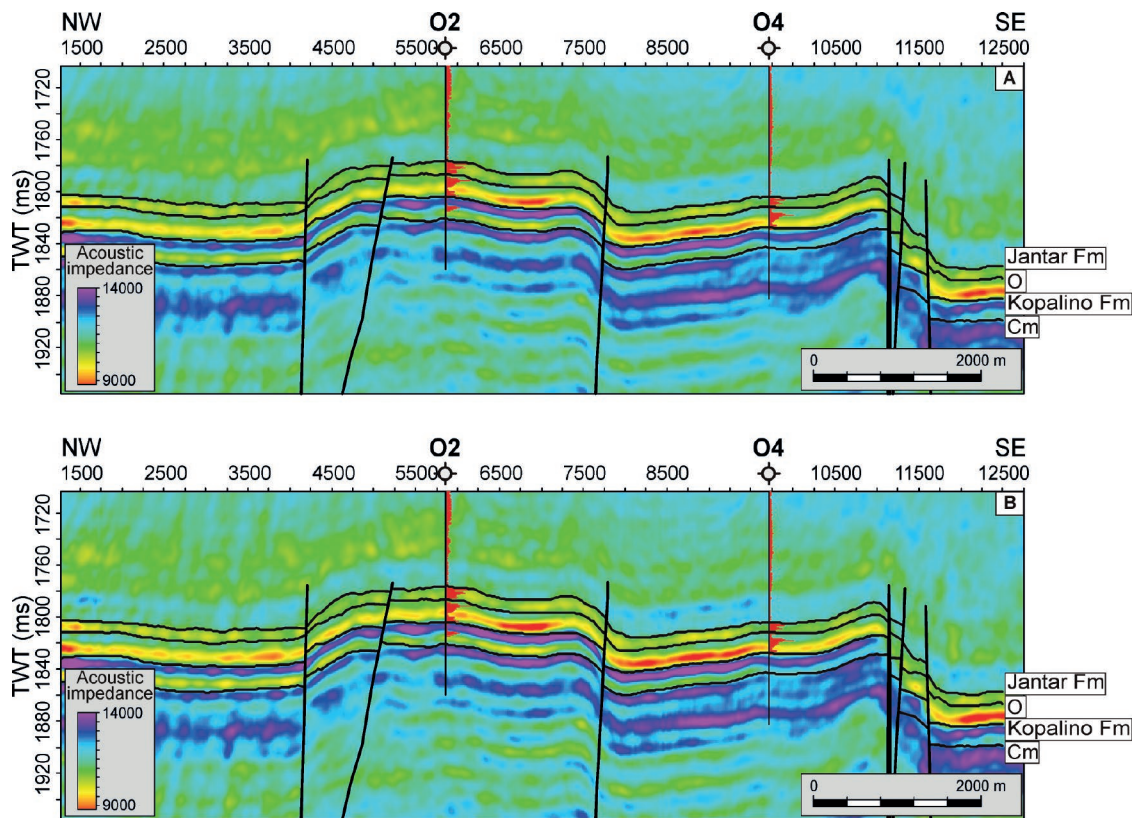
Fig. 20. Segment of an arbitrary seismic profile between wells O2-O4 after acoustic inversion. **A.** Original seismic data. **B.** After resolution enhancement with spectral blueing. Well data: VKER. O – top of Ordovician, Cm – top of Cambrian; after Cichostępski *et al*. (2017).
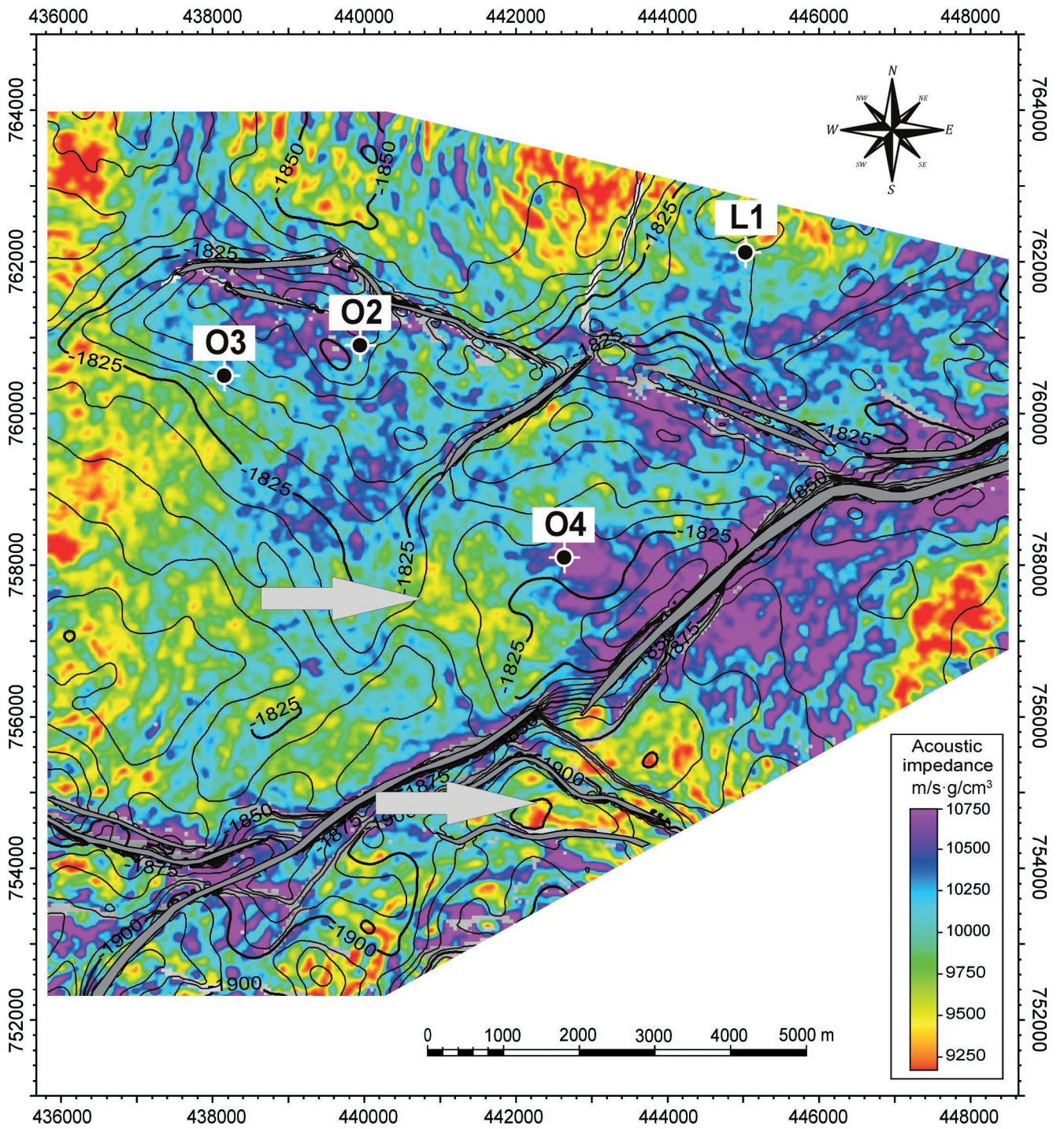
Fig. 21. The spatial distribution of acoustic impedance after resolution enhancement algorithm with the structural time map for the Jantar Formation. Arrows indicate potential sweet spots; after Cichostępski *et al.* (2017).

Fig. 22. The spatial distribution of acoustic impedance after resolution enhancement algorithm with the structural time map for the Sasino Formation. Arrows indicate potential sweet spots; after Cichostępski *et al*. (2017).

REFERENCES

Cichostępski, K. & Kasperska, M., 2016. Geomechanical properties of shale gas reservoirs in Poland Baltic Basin using AVO analysis and inversion. In: *78th EAGE Conference & Exhibition*, 30 May – 2 June 2016, Vienna, Austria: Extended Abstract. DOI: 10.3997/2214-4609.201601274.

Cichostępski, K., 2016. *Amplitude Versus Offset Analysis as a Tool for Identification of Gas Reservoirs in Thin Beds of the*

Carpathian Foredeep. Unpublished PhD Thesis, AGH-UST University of Science and Technology in Kraków, 212 pp. [In Polish.]

Cichostępski, K., Dec, J. & Kwietniak, A., 2019. Relative amplitude preservation in high-resolution reflection seismic: a case study from Fore-Sudetic Monocline, Poland. *Acta Geophysica*, 67: 77–94.

Cichostępski, K., Kwietniak, A., Kasperska, M., Dec, J. & Pietsch, K., 2017. Próba identyfikacji *sweet spotów* na podstawie zintegrowanych badań geofizycznych. In: Golonka, J. & Bębenek, S. (eds), *Opracowanie map zasięgu, biostratygrafia utworów dolnego paleozoiku oraz analiza ewolucji tektonicznej przy krawędziowej strefy platformy wschodnioeuropejskiej dla oceny rozmieszczenia niekonwencjonalnych złóż węglowodorów*. Wydawnictwo Arka, Cieszyn, pp. 472–493. [In Polish.]

Goodway, B., Chen, T. & Downton, J., 1997. Improved AVO fluid detection and lithology discrimination using Lamé petrophysical parameters: "λρ", "μρ", & "λ/μ fluid stack" from P and S inversions. *SEG Technical Program Expanded Abstracts*, 1997: 183–186.

Goodway, B., Perez, M., Varsek, J. & Abaco, C., 2010. Seismic petrophysics and isotropic-anisotropic AVO methods for unconventional gas exploration. *The Leading Edge*, 29: 1500–1508.

Gray, D., Anderson, P., Logel, J., Delbecq, F., Schmidt, D. & Schmid, R., 2012. Estimation of stress and geomechanical properties using 3D seismic data. *First Break*, 30: 59–68.

Hampson, D. & Galbraith, M., 1981. Wavelet extraction by sonic-log correlation. *Canadian Journal of Exploration Geophysics*, 17: 24–42.

Hampson, D. P., Russell, B. H. & Bankhead, B., 2005. Simultaneous Inversion of Pre-stack Seismic Data. *SEG Technical Program Expanded Abstracts*, 2005: 1633–1637.

Kasina, Z., 1998. *Processing of Seismic Data*. Wydawnictwo Centrum PPGSMiE PAN, Kraków, 333 pp. [In Polish].

Kiersnowski, H., 2013. Geological environment of gas-bearing shales. In: Nawrocki, J. (ed.), *Shale Gas as Seen by Polish Geological Survey*. Polish Geological Institute – National Research Institute, Warsaw, pp. 26–31.

Kwietniak, A., Cichostępski, K. & Pietsch, K., 2018. Resolution enhancement with relative amplitude preservation for unconventional targets. *Interpretation*, 6: SH59–SH71.

Latimer, R. B., Davison, R. & Van Riel, P., 2000. An interpreter guide to understanding and working with seismic derived acoustic impedance data. *The Leading Edge*, 19: 242–256.

Lindseth, R. O., 1979. Synthetic sonic logs – A process for stratigraphic interpretation. *Geophysics*, 44: 3–26.

Løseth, H., Wensaas, L., Gading, M. & Spronger, M., 2011. Can hydrocarbon source rock be identified on seismic data? *Geology*, 39: 1167–1170.

Pendrel, J., 2006. Seismic inversion – still the best tool for reservoir characterization. *Canadian Society of Exploration Geophysics Recorder*, 26: 5–12.

Poprawa, P., 2010. Shale gas potential of the Lower Palaeozoic complex in the Baltic and Lublin-Podlasie basins (Poland). *Przegląd Geologiczny*, 58: 226–249. [In Polish.]

Russell, B., 1988. *Introduction to Seismic Inversion Methods*. Course Notes Series, 2, Society of Exploration Geophysicists, 178 pp.

Veeken, P. C. H. & Da Silva, M., 2004. Seismic inversion methods and some of their constraints. *First Break*, 22: 47–70.

Walden, A. T. & Hosken, J. W. J., 1985. An investigation of the spectral properties of primary reflection coefficients. *Geophysical Prospecting*, 33: 400–435.

Widess, M. B., 1973. How thin is thin bed? *Geophysics*, 38: 1176–1180.

Zeng, H. & Marfurt, K. J., 2015. Recent progress in analysis of seismically thin beds. *Interpretation*, 3: SS15–SS22